On the stability of deep-seated landslides. The cases of Vaiont (Italy) and Shuping (Three Gorges Dam, China)

C. Seguí[1], H. Rattez[1], and M. Veveakis[1]

[1]Civil and Environmental Engineering Department, Duke University, Durham, USA.

Corresponding author: Carolina Seguí (carolina.segui@duke.edu)

Abstract

Deep-seated catastrophic landslides are among the most powerful natural hazards on earth. These devastating events are not possible to be prevented yet, because of their large volumes and sudden acceleration phase. The present study suggests a new method to detect when a landslide will turn unstable, giving both a time-window to evacuate the area that is going to be affected and critical values for measurable variables (velocity and basal temperature) up to which remediation measures can be deployed. This work focuses on large ancient landslides reactivated due to human interaction, like the construction of a dam in the vicinity of the landslide that causes water table variations and affects the stability of the landslide. The main hypothesis of this work is that most of the deformation of deep-seated landslides is concentrated on a thin, basal shear-band forming the sliding surface. That allows deep-seated landslides to be approximated as elastic/rigid blocks sliding over a viscoplastic shear band, featuring weak phases like expansive clays. When the landslide creeps, it causes friction in the shear band to raise the temperature and increase the pore pressure of the clays until they reach a point of near-zero friction and collapse catastrophically. This study deploys an energy-based approach, accounting for the heat generated due to friction, to find the critical point where the landslide turns unstable. The theoretical model consists in a stability analysis of the landslide using a pseudo-arclength continuation method. The model is applied to the famous Vaiont landslide in Northern Italy and Shuping landslide in Three Gorges Dam in China. The results of the model reproduce with great accuracy the behavior of both landslides, thus, finding the critical point of stability of the slide.

Keywords: Creep, Friction, Groundwater, Landslides, Shear Strength, Temperature Effects

1 Introduction

Massive, deep-seated and catastrophic landslides are usually preceded by prolonged periods of accelerating creep, and they frequently involve almost rigid volumes of rock mass (~10^6-10^7 m^3) creeping over a thin, basal shear zone, under total loads of ~ 1-10 MPa [*Kilburn and Petley, 2003*]. In order to provide rational explanation of the unexpectedly high velocities (with respect to the creeping velocities) that these landslides achieve during their very last phase, *Habib* [*1967*] first suggested the vaporization concept. According to Habib, mechanical energy dissipated in heat inside the slip zone may lead to vaporization of pore water, thus creating a cushion of zero friction. Using one-dimensional analysis of sliding-block mechanisms it was first *Anderson* [*1980*] and later *Voight and Faust* [*1982*] who showed that even if vaporization does not take place in a slide, heat generation may cause high pore pressures to develop at some stage inside the shear band. These mechanisms are nowadays accepted in the fault mechanics community, which dealt with the problem of pore-fluid pressures and frictional heating [*Lachenbrunch, 1980*] as well as frictional melting in relation to the seismic fault rapture [*Mase & Smith, 1984*]. Indeed, *Rice* [*2006*] claimed the onset of thermal pressurization as the primary fault weakening mechanism during coseismic slip.

Veveakis et al. [*2007*] used a simple, one dimensional model of a rigid block sliding over a clay-rich zone of intense shear to show that the prolonged creep of a slide might trigger excess pore-pressure generation due to the friction-induced temperature rise (i.e. thermal pressurization). Past this point, the phenomenon evolves explosively, until the moment where the pore pressure reaches its maximum value (the value of the normal stress) and the strength of the gouge drops to zero, explaining the catastrophic accelerations that these landslides obtain during their final collapse [*Vardoulakis, 2002a*]. The model was used in the case of the infamous Vaiont slide (located in the Northern Italian Alps), assuming that the applied shear stress remained constant and excluding any influence of the pore-pressure due to the underground water table variations. Even with the over-simplifying assumption of ignoring the temporal influence of the ground water level, the model managed to reproduce the velocity data provided by *Müller* [*1964, 1968*] for the last 169 days before the final collapse of the slide.

The aforementioned analysis [*Veveakis et al., 2007*] verified the claim that the thermal pressurization mechanism can indeed be considered to be the mechanism that dominates the final catastrophic phase of the slide [*Vardoulakis, 2002a, Pinyol and Alonso, 2010,* and *Cecinato et al., 2011*]. However, it revealed also the fact that thermal pressurization is not the primary mechanism that turns a creeping landslide unstable. Indeed, the calculations revealed that the process became unstable long before thermal pressurization was triggered, when the heat diffusion inside the basal shear zone was changed from normal diffusion to the unstable uphill diffusion [*Veveakis et al., 2007*]. This critical time of this transition was identified as the point that the heat diffusion in the shear zone starts localizing in a continuously shrinking shear zone, causing essentially adiabatic conditions inside the shear band and thus increasing abruptly the temperature of the shear zone.

In this paper we will extend the study of *Veveakis et al.,* [*2007*], to account for the effect of evolving groundwater table, both by precipitation and reservoir levels. In doing so, our goal is to reveal whether this critical threshold, apart from being the point where stable diffusion becomes unstable, can be also considered as a stability threshold for deep-seated landslides. To achieve that, we will try to reproduce the history of the Vaiont slide during the 2 years of its movement and the history of the Shuping slide during the 10 years of its movement, and determine the points of instability for each case.

2 Multi-scale model of a deep-seated landslide

In order to model deep-seated landslides, we use a model incorporating configurations at three different scales, as initially suggested by *Vardoulakis,* [*2002a*] and is shown in Figure 1. In particular, we use A) a *static configuration*, whereby using the “real” topography we calculate the groundwater table of the landslide and therefore the shear stress experienced on the sliding surface; (B) a *kinematic configuration*, where the landslide topography is mapped into the equivalent kinematic space where its displacement is being solved for: circular for rotational landslides and infinite plane for translational ones; and (C) the *shear-band configuration*, where all the physical mechanisms admitted by the material are constituting a multi-physics mathematical configuration. In this work we will focus on translational landslides (i.e. the kinematic configuration is an infinite plane) and on the thermo-poro-mechanical behavior of the material in the shear-band. In the following paragraphs we explain how each configuration is approached and linked with the others.

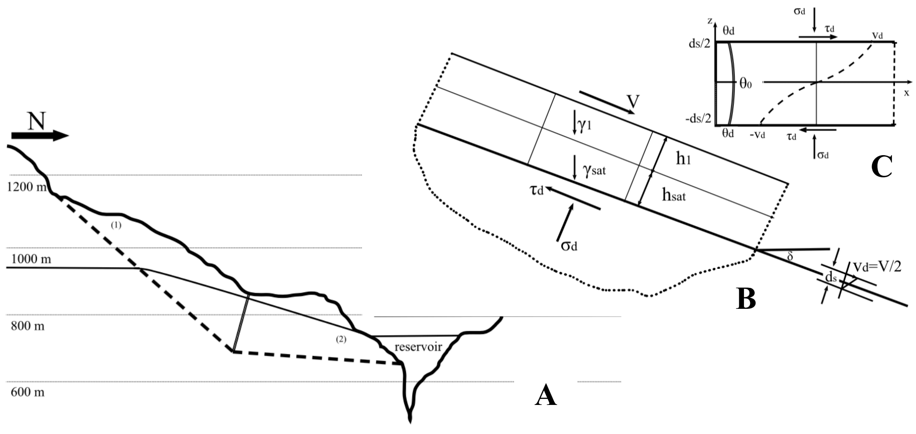

Figure 1. Multi-scale model of a deep-seated landslide. **A)** Static configuration: Topographic cross-section of the landslide in which classical stress calculations are performed. **B)** Kinematic configuration: The landslide is treated as translational, with its kinematics represented as an infinite rigid-elastic block sliding over a shear band. **C)** Shear band configuration: The shear band of the landslide incorporating thermo-mechanical couplings [*Veveakis et al, 2007*].

2.1 Groundwater table of a landslide

We start by calculating the stresses acting on the sliding surface, through a hydro-mechanical analysis of the landslide at the *static configuration* level. For this, we need two elements: the groundwater table and the forces acting inside the landslide. To study the groundwater table of a landslide we use the topographic cross section of the scale (A) in Figure 1 and calculate the hydraulic head (h) at each point of the landslide using Darcy's law (Equation 1) and assuming: 1) horizontal flow, 2) constant Darcy velocity in the horizontal direction, 3) the presence of a free aquifer in the landslide, and 4) that the groundwater discharge is proportional to the saturated aquifer thickness. These assumptions allow us to consider Darcy's law in one dimension as representative of the fluid flow discharge:

$$q = -K\frac{dh}{dl} \tag{1}$$

where q is the specific discharge [L/T], K is the hydraulic conductivity [L/T], $\frac{dh}{dl}$ is the hydraulic gradient, h is the hydraulic head [L], and l is the horizontal length of interest [L].

Considering the above assumptions, the final equation of the water table at each time step consists of the mass balance equation, written for the hydraulic head [see *Craig, 2004*],

$$\frac{\partial h}{\partial t} = D\frac{\partial^2 h}{\partial x^2} \tag{2}$$

where D is the diffusivity [m^2/s], and the hydraulic head is related to the pore fluid pressure P_f as $h = \frac{P_f}{\rho g} - z$. Equation (2) is solved analytically, with appropriate boundary conditions,

$$\begin{cases} x = x_1 \rightarrow h = H_1 \\ x = x_2 \rightarrow h = H_2 \end{cases} \tag{3}$$

to obtain:

$$h = \frac{(H_1 - H_2)\,\mathrm{erf}\left(\frac{\xi}{2}\right) + H_2\,\mathrm{erf}\left(\frac{\xi_1}{2}\right) - H_1\,\mathrm{erf}\left(\frac{\xi_2}{2}\right)}{\mathrm{erf}\left(\frac{\xi_1}{2}\right) - \mathrm{erf}\left(\frac{\xi_2}{2}\right)} \quad (4)$$

where $\xi_i = \frac{x_i}{2\sqrt{kt}}$, and *erf* is the error function. This is therefore the equation for the hydraulic head inside the body of the slope, given 2 values (through piezometers or lake elevation) at selected points x_1 and x_2. In the next section, we'll use this information to calculate the stresses acting on the sliding surface of a landslide.

2.2 Force equilibrium and Coulomb mechanism of a landslide

Once the groundwater level of the landslide has been calculated, we calculate the shear stress of the landslide depending on the groundwater level at the *static-configuration* scale (A) in Figure 1. Firstly, we consider calculating the forces of the landslide using the two-wedge method [*Alonso, 1989*] in which the equilibrium forces are calculated separately for each wedge, and after that we calculate the shear stress as a mean between the two blocks to obtain the total shear stress of the landslide [*Alonso and Pinyol, 2010*]. Thus, we divide the landslide into two blocks based on the topography, therefore setting the division line that separates the landslide in two blocks where the interface layer changes the slope at the bottom, and where the topography changes the slope drastically at the top (Figure 2). It is to be noted that the two-wedge method is just one of the available force equilibrium approaches (others being the Fellenius or Bishop method of slices, etc), and is used here for simplicity in the mathematical treatment.

We consider that the Wedge 1 acts on the Wedge 2 as an active force, and the Wedge 2 acts on the Wedge 1 as a passive force. The type of Coulomb's lateral pressure of each wedge has been considered as active the wedge that has a higher slope to the horizontal in the shear band, and as passive the wedge that has a lower slope in the shear band to the horizontal. Figure 2 shows the forces acting on each wedge of a landslide.

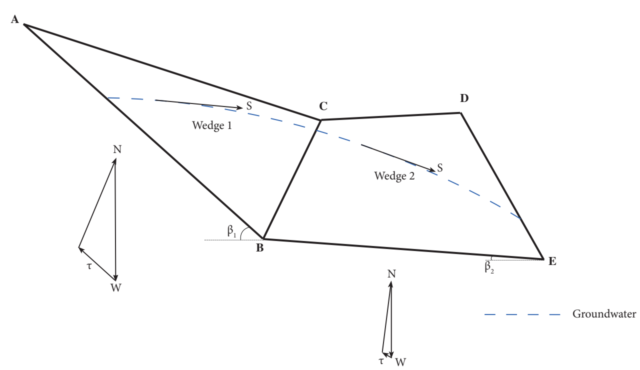

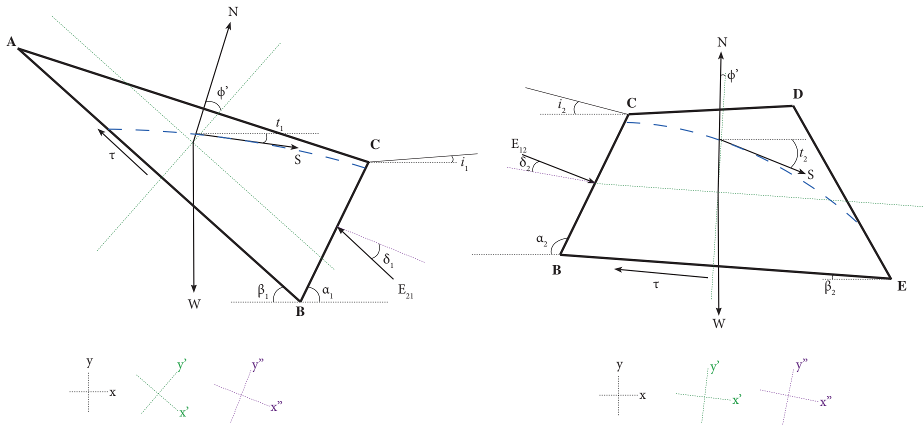

Figure 2. Top: Section profile of a deep-seated landslide with a two-wedge mechanism and its force equilibrium. Bottom: the forces acting on each of the two wedges

The equations of each force acting on Wedge 1 and Wedge 2 are the weight and seepage. The weight W [kN] of each wedge is calculated as:

$$W = \gamma_{sat}\ Area_{sat} + \gamma_{dry}\ Area_{dry} \tag{5}$$

where γ_{dry} is the specific unit weight of the soil [kN/m^3], which is the difference between γ_{sat} (specific unit weight of saturated soil [kN/m^3]) and γ_w (specific unit weight of water [kN/m^3]), $Area_{sat}$ is the area of saturated soil [m^2], and $Area_{dry}$ is the area of dry soil [m^2]. The seepage force [KN/m] is acting as a positive force on each wedge, and is calculated as:

$$S = Area_{sat}\ \gamma_w \tag{6}$$

Applying the earth pressure theory of Rankine [see chapter 11 of *Craig, 2004*], we can calculate the active and passive forces of the landslide as follows. The active force is:

$$E_{12} = \left(0.5\ \gamma_{sat}\ H_{sat}^{\ 2}\ k_a - 2\ c\ H_{sat}\ \sqrt{k_a}\right) + \left(0.5\ \gamma_{dry}\ H_{dry}^{\ 2}\ k_a - 2\ c\ H_{dry}\ \sqrt{k_a}\right) \tag{7}$$

where E_{12} is the active earth force [KN] acting in the Wedge 2 as positive, H_{sat} and H_{dry} are the normalized heights of saturated soil and dry soil [m], respectively, at the interface line between the two wedges, c is the cohesivity [KN/m^2], and k_a is the active lateral earth pressure coefficient [-] calculated as follows by Rankine's theory:

$$k_a = \frac{\sin^2(\alpha_1 + \phi)}{\sin^2\alpha_1\ \sin(\alpha_1 - \delta_2)[1 + \sqrt{\frac{\sin(\phi + \delta_2)\sin(\phi - \beta_2)}{\sin(\alpha_1 - \delta_2)\sin(\alpha_1 + \beta_2)}}]} \tag{8}$$

with α_1 being the angle of the interface line that divides the two blocks with the horizontal [°], ϕ the friction angle [°], δ_2 is set at 2/3 of the friction angle [°], and β_2 the angle of the topography of the Wedge 2 against the horizontal [°].

The passive earth force E_{21} [KN] acting in the Wedge 1 is, respectively:

$$E_{21}=\left(0.5\ \gamma_{sat}\ H_{sat}^2\ k_p - 2\ c\ H_{sat}\sqrt{k_p}\right)+\left(0.5\ \gamma_{dry}\ H_{dry}^2\ k_p - 2\ c\ H_{dry}\sqrt{k_p}\right) \tag{9}$$

where k_p is the passive lateral earth pressure coefficient [-], calculated as follows by Rankine's theory:

$$k_p=\frac{\sin^2(\alpha_2-\phi)}{\sin^2\alpha_2\sin(\alpha_2+\delta_1)[1-\sqrt{\frac{\sin(\phi+\delta_1)\sin(\phi+\beta_1)}{\sin(\alpha_2+\delta_1)\sin(\alpha_2+\beta_1)}}]} \tag{10}$$

In this expression α_2 is 180 minus α_1 [°], δ_1 is 1/3 of the friction angle [°], and β_1 is the angle of the topography of the Wedge 1 with the horizontal [°].

Thus, the horizontal equilibrium forces acting on Wedge 1 is as follows:

$$\tau + E_{21_H} - S\cos(\beta_2-\alpha_2) + N\sin(\varphi') - W\cos(\beta_2) = 0 \tag{11}$$

where N is the normal force acting as positive on both wedges [KN], τ is the shear stress force [KN] acting at the bottom of the wedge as negative on both wedges, β_2 is the angle of the slope of the Wedge 2 with the horizontal [°], $\alpha_2[°]=\frac{\beta_2+t_2}{2}$ where t_2 is the angle of the slope of the water table with the horizontal [°] at Wedge 2, and φ' is the friction angle of the soil [°].

Correspondingly, horizontal force equilibrium for the Wedge 2 reads:

$$\tau - E_{12_H} - S\cos(\beta_1-\alpha_1) + N\sin(\varphi') - W\cos(\beta_1) = 0 \tag{12}$$

where β_1 is the angle of the slope of the Wedge 2 with the horizontal [°], and $\alpha_1[°]=\frac{\beta_1+t_1}{2}$ where t_1 is the angle of the slope of the water table with the horizontal [°] at Wedge 1.

The vertical equilibrium forces acting on Wedge 1 (Equation 13) and on Wedge 2 (Equation 14) are as follows:

$$N\cos(\varphi') - W\sin(\beta_2) + S\sin\left(\beta_2-\alpha_2\right) + E_{21_V} = 0 \tag{13}$$

$$N\cos(\varphi') - W\sin(\beta_1) + S\sin\left(\beta_1-\alpha_1\right) - E_{12_V} = 0 \tag{14}$$

Thus, we can calculate the normal (N) and shear (S) forces of each wedge from the above four last equations (Equations from 11 to 14). By then dividing S with the area L (assuming unit length in the third direction) of the sliding surface, we calculate the mean basal shear stress force for the landslide [*Muller, 1968*] as follows:

$$\bar{\tau}_d = \frac{1}{h^{(1)}+h^{(2)}} \left(h^{(1)}\tau_d^{(1)}+h^{(2)}\tau_d^{(2)}\right) \tag{15}$$

In this expression, $\bar{\tau}_d$ is the mean (at the center of mass) shear stress of the landslide [MPa], $h^{(1)}$ is a normalized height [m] of dry soil height plus saturated soil height of Wedge 1, $\tau_d^{(1)}$ is the shear stress of Wedge 1 [KN], $h^{(2)}$ is a normalized height [m] of dry soil height plus saturated soil height of Wedge 2, and $\tau_d^{(2)}$ is the shear stress of Wedge 2 [KN].

2.3 Thermo-poro-mechanic behavior of the shear band

After calculating the stresses acting on the landslide, we move to the model presentation of the 1D rigid-block/shear-band approach. We are briefly presenting the conceptual model used in the paper of *Veveakis et al* [*2007*] in order to model such a deep-seated landslide, incorporating the *kinematic configuration* and *shear-band configuration* scales, as shown in Figure 1B and 1C. As such, a translational landslide is approached as an infinite rigid-elastic block sliding over a thin layer of clay (i.e. the shear zone). The slope where the infinite rigid-elastic block is sliding, has been considered as a mean between the slopes of the two-wedges of the landslide, so that the dynamics of the landslide are respected [see *Veveakis et al*, *2007*]. Because the block is assumed rigid, the velocity along the vertical axis of the infinite block is constant. The rigid-elastic block therefore admits the shear-stresses calculated in the previous section (2.2) in its center of mass, and applies them on the shear band.

The clay material inside the shear zone was assumed to be at critical state at every variation of groundwater table, deforming thus under constant volume at each time step. This assumption is therefore rendering any volumetric effects negligible [see *Veveakis and Regenauer-Lieb, 2015*], based on the acceptance that clays reach critical state upon relatively small displacements when sheared [*Tika and Hutchinson*, *1999*]. The shear zone material was assumed to be always fully saturated in water and the various mechanical fields vary along the sort z-axis, establishing a single dimension model. The behavior of the clay material in the shear zone has been considered to exhibit thermal and rate sensitivity, following the work of *Vardoulakis*, [*2002a*]. The clays do not have a constant behavior, they are exhibiting velocity hardening meaning that the strain-rate increases when the shear stress rises, and thermal softening, implying that when the temperature in the clays increases the friction coefficient of the material decreases.

Thus, the friction coefficient at critical state (Equation 16) can be defined as a multiplication between velocity hardening and thermal softening, being a combination of a power law and an exponential law:

$$\mu_{cs} = g(\dot{\gamma}) \cdot f(\theta) = \mu_{ref} \left(\frac{\dot{\gamma}}{\dot{\gamma}_{ref}}\right)^N e^{-M(\theta-\theta_1)} \tag{16}$$

where μ_{cs} is the critical friction coefficient [-], μ_{ref} is the reference friction coefficient [-], $\dot{\gamma}$ is the shear strain-rate [-], $\dot{\gamma}_{ref}$ is the reference strain-rate [-], N is the frictional rate-sensitivity coefficient [-], M reflects the temperature dependence of water viscosity [-], θ_1 is the temperature reference [°C], and θ is the actual temperature in the shear band [°C].

Considering that the friction coefficient at critical state is defined as $\mu_{cs} = \frac{\tau}{\sigma_0}$, where τ is the shear stress and σ_0 is the normal stress, we may assume the shear band material to be perfectly viscoplastic to solve Eq. (16) for the shear strain rate:

$$\dot{\gamma} = \dot{\gamma}_0 \left(\frac{\tau}{\sigma_n}\right)^{1/N} e^{m(\theta-\theta_1)}, \quad m = \frac{M}{N} \tag{17}$$

where $\dot{\gamma}_0$ is the reference shear strain rate of the shear zone [s^{-1}], σ_n is the normal stress [KN], *m* is the exponent ratio of the temperature sensitivity coefficient over the strain rate sensitivity coefficient [$°C^{-1}$]. Note that the exponential dependency on temperature, shown in Eqs. (16-17), corresponds to the low-temperature approximation of the more generic Arrhenius law, as used in the same mechanical considerations for the mechanics of faults, at deeper (abd therefore higher temperature) environments than landslides [*Alevizos et al, 2014; Veveakis et al., 2014; Poulet et al, 2014*].

Having established the constitutive law for the basal material, the mathematical model of the shear-band [see *Veveakis et al*., *2007*, for a detailed description] comprises: 1) the heat diffusion equation for local entropy production:

$$\rho C \frac{\partial \theta}{\partial t} = k\nabla^2\theta + \tau\,\dot{\gamma} \tag{18}$$

where ρC is the specific heat of the mixture [J (Kg °C)$^{-1}$], k is the Fourier's thermal conductivity of the clay [cal (°C m s)$^{-1}$], and $\tau\,\dot{\gamma}$ is the plastic stress power; and, 2) the momentum balance for clay in one dimensional simple shear for each direction:

X direction: $\frac{\partial \sigma_{xy}}{\partial y} = 0$, thus $\sigma_{xy} = \tau_d$ (19)

Y direction: $\frac{\partial \sigma_{yy}}{\partial y} = 0$, thus $\sigma_{yy} = \sigma_n$ (20)

The governing equations (18,19,20), together with the constitutive law of Eq. (17), are combined in a single equation, that is brought in dimensionless form using the following scalings:

$$z^* = \frac{z}{\left(\frac{ds}{2}\right)}, \qquad t^* = \frac{k_m}{\left(\frac{ds}{2}\right)^2} t, \quad \theta^* = m(\theta - \theta_1) \tag{21}$$

In these equations ds is the real thickness of the shear band [m], z is the thickness of the shear band from Figure 1C [m], k_m is Kelvin's coefficient of thermal diffusivity of the soil-water mixture [m^2/s], and *t* is time [s].

Following this scaling, Equations (17-20) can be combined in a single dimensionless equation describing the thermo-mechanical response of the basal material, as follows:

$$\frac{\partial \theta^*}{\partial t^*} = \frac{\partial^2 \theta^*}{\partial z^{*2}} + \mathrm{Gr}\, e^{\theta^*}, \quad z \in [-1,1], \quad t>0 \tag{22}$$

In this expression, Gr is the so-called Gruntfest number [-],

$$\mathrm{Gr} = \mathrm{m}\frac{\dot{\gamma}_0}{\mathrm{jk_m}}\left(\frac{\mathrm{ds}}{2}\right)^2 \sigma_{ref}\left(\frac{\tau_d}{\sigma_{ref}}\right)^{1+1/N}, \tag{23}$$

where j is the mechanical equivalent of heat [J/kcal], and $\bar{\tau}_d$ depends on the lake water level variations [KN]. The Gruntfest number was originally suggested by *Gruntfest* [*1963*] and is expressing the ration of the mechanical work converted into heat over the heat diffusion capabilities of the material. It includes all the material properties at hand (thermal conductivity, rate and thermal sensitivities, and reference rate), as well as the thickness of the shear band and the normal and shear stresses applied on it. Since these stresses are calculated in the previous sections to be evolving with the groundwater level, *Gr* is in principle not constant in time. Therefore, in our analysis we will be calculating the Gruntfest number and the temperature at each time step (i.e. for each groundwater table).

3 Stability analysis of a deep-seated landslide

Having established the governing equation in the shear band, and before moving into transient considerations, we need to assess the stability of its long-term behavior. This is achieved by performing a numerical bifurcation analysis of the steady state of Equation (22),

$$\frac{\partial^2\theta^*}{\partial z^{*2}} + \mathrm{Gr}\ \mathrm{e}^{\theta^*} = 0, \tag{24}$$

with respect to the only free parameter of the problem, the Gruntfest number *Gr*. The numerical bifurcation is performed by using a pseudo arc-length continuation approach [*Chan and Keller, 1991*, *Veveakis et al, 2010*].

The results of this analysis are presented in Figure 3a, where the maximum value of the dimensionless temperature solution of the steady state equation (Equation 24) is plotted for every value of the bifurcating parameter *Gr*. We notice the presence of 2 steady state solutions for values of the *Gr* lower than its critical value of Gr_c~0.88, one at the turning point (black dot) where $\mathrm{Gr} = \mathrm{Gr_c}$, and no steady state solutions when $\mathrm{Gr} > \mathrm{Gr_c}$. The lower branch is a stable attractor of the transient system, whereas the upper branch is unstable [see also *Veveakis et al, 2010*]. These results therefore delimit the stable area of our system to be the highlighted grey area of Fig. 3A. Should the system be somehow pushed outside this area, a catastrophic infinite increase of the temperature will occur, a response known in the literature as blow-up instability [*Veveakis et al, 2007*].

To showcase this response in terms of both temperature and velocity evolution inside the shear band, we select two points as initial conditions (points 1 and 2 in Fig. 3A). Starting at point 1, which is at a Gruntfest value below the critical point (Figure 3a), the temperature and velocity will stabilize over time (Figure 3B and 3C). This means that indeed when the Gruntfest number of the landslide is located below the turning point, the slope would be creeping in a stable manner. However, starting at point 2, at a Gruntfest value above the critical point (in Figure 3A), the temperature and velocity increase exponentially (i.e. blow-up) over time (Figure 3B and 3C), leading the landslide to collapse catastrophically in finite time.

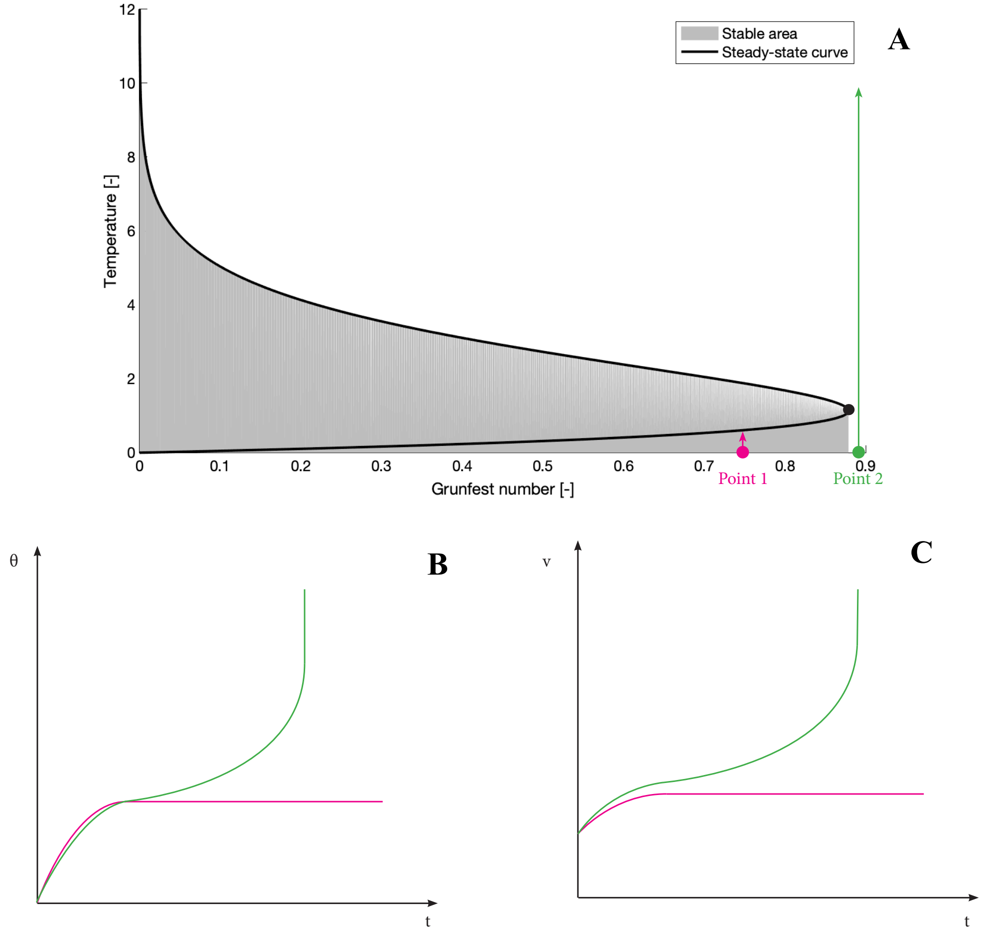

Figure 3. A) Steady-state curve with its critical point (black dot), stable point 1 (pink dot and arrow), and unstable point 2 (green point and arrow). **B)** Representation of the stable and unstable points from Figure 3A in terms of temperature versus time. **C)** Representation of the stable and unstable points from Figure 3A in terms of velocity versus time.

This analysis highlights the crucial role of the Gruntfest number in the stability of the system, suggesting that it is the driving factor for the stability of a landslide. As already discussed, *Gr* is unlikely to be constant over time, as it incorporates the loading conditions (shear and normal stresses) of the landslide:

$$Gr = m\,\tau_{(1,1)}\,\dot{\gamma}_0\,\frac{\frac{ds^2}{4}}{jk_m}\,\tau^{1+\frac{1}{N}} \tag{25}$$

Recall that in this expression, τ is the shear stress in dimensionless form [-], and $\tau_{(1,1)}$ is the initial value of the shear stress [-].

Using this definition of the Gruntfest number, and the values of the shear stress calculated through our groundwater analysis (Equations 1 to 4) we expect to be able to determine the stability threshold of a landslide through this bifurcation analysis. To assess this claim, in the next sections we apply the model to two case studies with different behaviors: 1) the Vaiont landslide in Italy, which turned unstable after years of slow creep and failed catastrophically; and 2) the Shupping landslide in China which creeps stably for decades.

4 Case of study: Vaiont landslide

The famous Vaiont landslide (Figure 4A and 4B) occurred in October 9th of 1963 in Northern Italy. It has been reported in literature as an ancient landslide that reactivated when the Vaiont dam was built and started filling the reservoir in 1959 [*Semenza and Melidoro, 1992*]. Recent studies [*Dykes and Bromhead, 2018a,b*] suggest that the final catastrophic landslide could be seen as a first time event, in which case the 3 years of creep would only contribute to the landslide progressively losing its structural strength and the dolomite layers to crack forming a weak shear band. Although theoretically possible, such a mechanism cannot be validated or invalidated by current field evidence or existing data collected from the site. As such, in this work we will assume that the landslide is a reactivation, allowing us to set the basal material at critical state and deploy the suggested framework.

During this period of 3 years that the landslide was creeping, the lake level fluctuated depending on the season of the year, from 590 to 710 meters (Figure 4E). Due to the fact that the landslide was instrumented, it had been seen that the velocity of the slide increased when the lake level rose. Therefore, the landslide was being stabilized by controlling the lake water level. However, in September 1st of 1963 the lake water level reached 710m and the slide started accelerating, and even though the water level was reduced in October 2nd of 1963 in order to stop the acceleration, the landslide accelerated until it became catastrophic. The thickness of this slide was about 150 m and a mass of $2.7x10^8$ m^3 of rock (Figure 4C). When the event occurred, the rock mass slide into the reservoir creating a wave over 200m height that overflowed the dam and caused 2000 casualties in the downstream valley.

4.1 Geographical location and geological framework

The Vaiont dam is situated in a steep valley in the Italian Alps, located under the Mount Toc in the Pordenone province, the region of Friuli-Venice Julia in Northern Italy (Figure 4A). The Piave river was crossing this valley and ending up in the Vaiont Lake. Upstream the river, the valley is wide due to it is a Glacial valley, and downstream the valley is narrower, which made it a very good location to build a dam. The stratigraphy of the area (Figure 4D) is composed of massive oolitic calcarenite from the Calcare of Vaiont formation, biocalcarenites and micritic limestone from the Fonzano formation, reddish and grey micrite with ammonites with thin layers of clays from Ammonitico Rosso formation, and intercalations of microcrystalline limestones, calcarenites and loam from the Calcare of Soccher formation of the Lower Cretaceous [*Ferri et al, 2011*].

Due to the fact that the mass of rock was sliding over clay layers, more detailed information of the clay layers is needed. These were a mixture of clays (Ca-montmorillonite, smectite, illite and vermiculite) with a 35 to 80% of content, and grains of calcite and minor quartz. These kinds of clays are frequently called “expansive clays” which have a low shear strength, expanding behavior, and in the presence of water they have a swelling response.

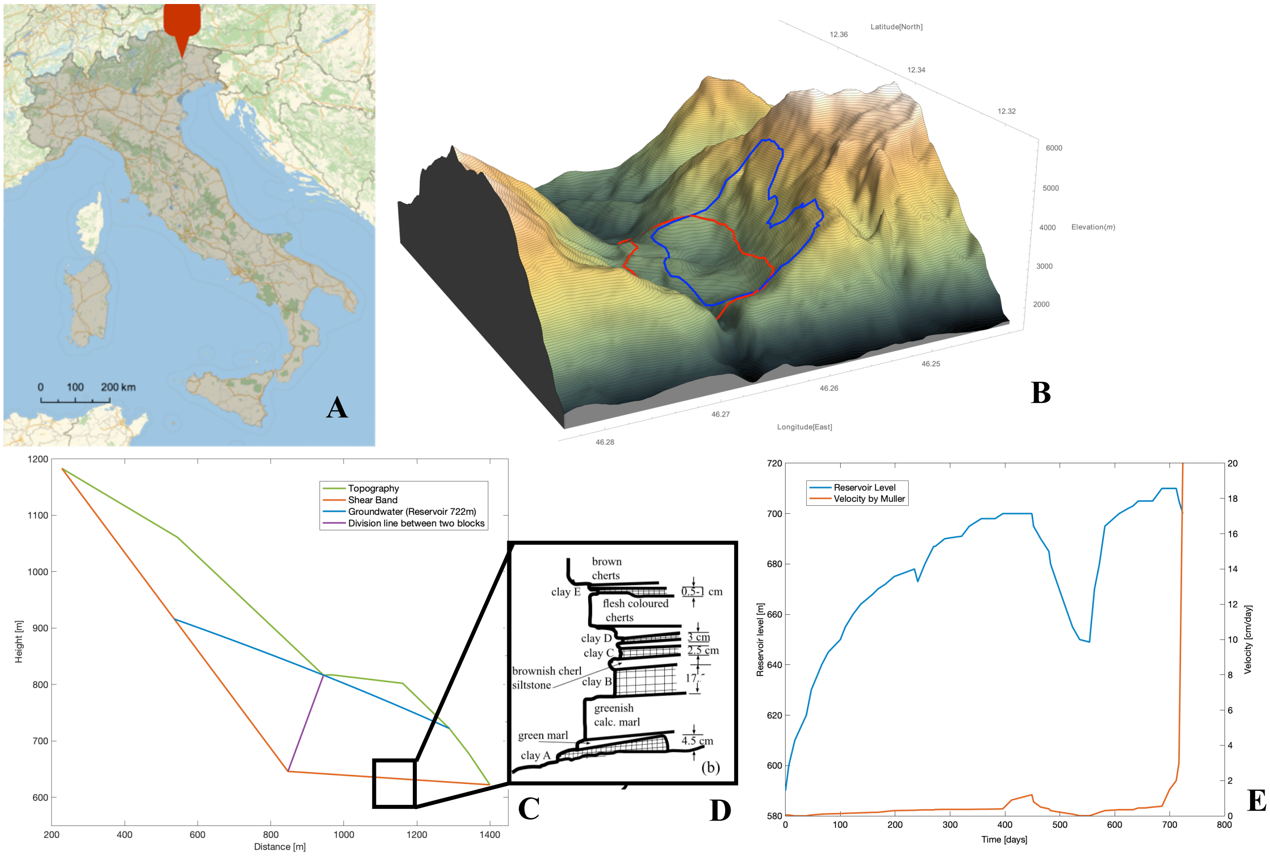

Figure 4. A) Map of location of the Vaiont dam. **B)** 3D elevation map of the Vaiont landslide (blue is the initial position of the mass, and red is the final position of the mass after the collapse). **C)** Profile of the deep-seated Vaiont landslide. **D)** Stratigraphic profile of the lithology of the Vaiont landslide [*Veveakis et al, 2007*]. **E)** Graph showing the reservoir level and the velocity of the landslide during the two years period of recording data [*Muller1964, 1968*].

4.2 Groundwater analysis

The groundwater table of the Vaiont landslide has been calculated considering that the dolomite is permeable enough to allow the groundwater to reach steady state in between the lake level variations. Thus, we calculate the groundwater level by setting Eq. (2) to steady state, therefore retrieving the Dupuit-Forchheimer parabola:

$$h=\sqrt{H_1^2-(H_1^2-H_2^2)\frac{x}{L}} \tag{26}$$

where h is the height of groundwater [m], H_1 is the height of water level of the reservoir [m], H_2 is the height of groundwater at the fixed point in the back of the landslide [m], L is the horizontal length between the point of reservoir in contact with the topography of the landslide and the fixed point in the back of the landslide [m], and x is the horizontal length along the landslide [m].

4.3 Shear stress results

Due to the lack of acceptable data of the piezometers [see *Hendron and Patton, 1985* for a comprehensive discussion on that], the underground water level is assumed to obtain always a high value, overestimating the mean basal shear stress by ~0.1 MPa during the periods of low precipitation and snowmelt. From the computed basis reaction forces, the mean values for the shear and normal effective stresses are computed. The considered mechanism (Section 2.2) yields estimate for the shear stress, the normal effective stress at the base of the slide and of the total mean height of the rigid block. Following the double wedge procedure described in section 2.2, and using the lake level data of Fig. 4E, a linear dependency between the lake level and the geostatic shear stresses is obtained.

$$\tau = 0.0017\ hl - 0.118 \tag{27}$$

where τ is the shear stress in MPa, and hl is the reservoir level in meters.

Thus, Figure 5A shows the shear stress [MPa] of all the reservoir levels [m] recorded for two years and calculated with Equation 27.

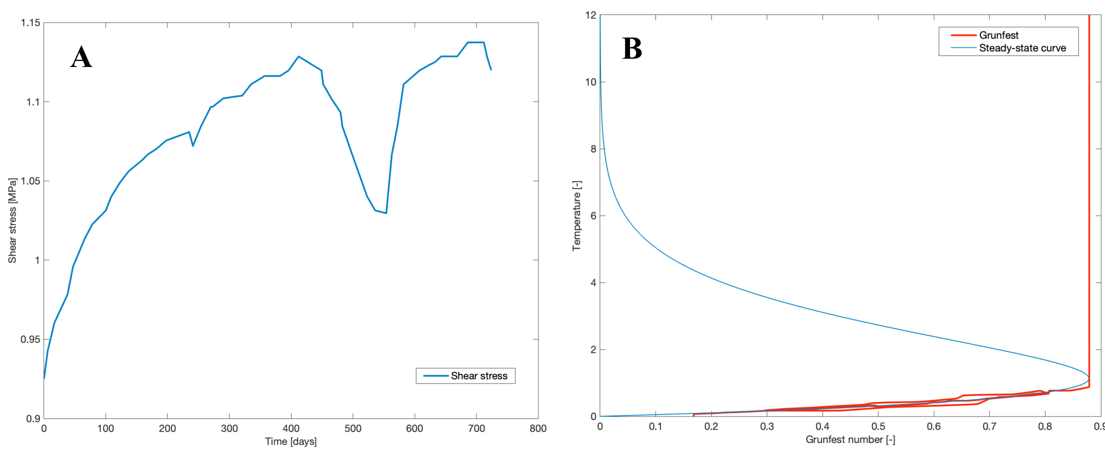

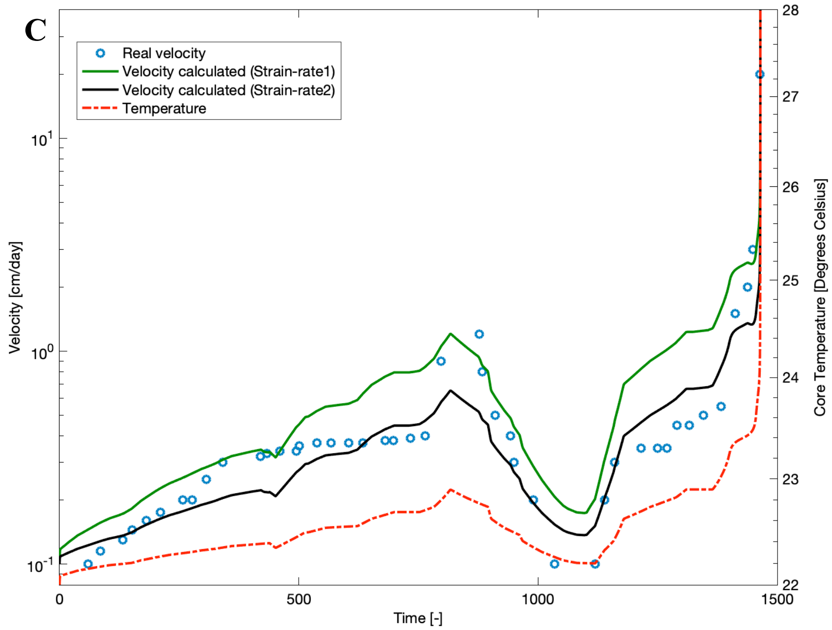

Figure 5. Results of the Vaiont slide: **A)** Graph that represents the shear stress value at each lake water level during the 2 years of recorded data of the Vaiont dam. **B)** Gruntfest number calculated versus temperature, with the stability curve. **C)** Velocity data from the field [M*üller, 1964*] as dots, two velocities calculated as lines, and dashed/dotted line as a temperature in the shear band.

As the results of our study, but also of *Vardoulakis* [*2002*], *Alonso and Pinyol* [*2010*], and *Dykes and Bromhead* [*2018*] suggest, taking into account only the variations of shear stresses (20% difference) is not enough to decrease the factor of safety of the landslide by 50%, which the factor of safety reduction required in order for the landslide to admit its final collapse. Alternative mechanisms are therefore sought for, in order for either the friction coefficient to decrease or the pore water pressure to increase and destabilize further the landslide. One can think of mechanisms like the presence of perched aquifers inside the limestone strata that are in turn formed by crack propagations, and that increase abruptly the pore water pressure during periods of heavy rainfall for the Vaiont landslide [*Dykes and Bromhead, 2018*]. Although plausible, this hypothesis is impossible to be corroborated in the field [*Dykes and Bromhead, 2018a* page 1826] or by laboratory experiments. Other hypotheses in the literature include various mechanisms for frictional weakening, including thermal pressurization of the clay layers triggered by frictional heating [*Lachenbrunch, 1980*], strain and strain rate softening [*Tika and Hutchinson*, *1999*; *Vardoulakis, 2002*], or thermal softening [*Veveakis et al, 2007, Veveakis et al, 2010*] that would reduce the frictional resistance of the slide by 50%. Since the effects of strain, strain rate and temperature can be validated by laboratory experiments [*Tika and Hutchinson*, *1999; Veveakis et al, 2010*], in this study we will focus on the combined effects of temperature and strain rate (velocity) on the friction coefficient.

4.4 Transient stability analysis

In order to calculate the velocity of the landslide and the Gruntfest number, we need the material parameters of the clay [*Veveakis et al, 2007*] that forms the shear band of Vaiont (Table 1).

Table 1. Material parameters of the gouge of Vaiont and Shuping landslides [*Veveakis et al, 2007*].

	Vaiont	Shuping	
Parameter	**Value**	**Value**	**Units**
m	56.62	0.6	$°C^{-1}$
ds	0.161	0.7	m
k_m	$1.6\cdot10^{-7}$	$1.6\cdot10^{-7}$	m^2/s
jk_m	0.45	0.45	$J\ (°C\ m\ s)^{-1}$
$\dot{\gamma}_{0_1}$	$3.34\cdot10^{-2}$	$50.59\cdot10^{-2}$	s^{-1}
$\dot{\gamma}_{0_2}$	$6.28\cdot10^{-2}$	$44.95\cdot10^{-2}$	s^{-1}
N	0.01	1	[-]
M	0.56	12	[-]
θ_1	22	-	°C
D	-	10	m^2/s

In this study case, the system calculated for the Vaiont landslide becomes unstable for a Gruntfest number of 0.88 and for a dimensionless temperature of 1.2 (Figure 5B). The velocity calculated for the Vaiont has been fitted for the field data [*Müller, 1964*]. In this case, for the velocity that we obtained with our calculations (Figure 5C) we needed to calculate two velocities to fit with more accuracy the velocity taken in the field.

As can be seen in Figures 4E and 5C, during the period of 2 years of data before the collapse of the landslide, the reservoir underwent through two vast embankments that the data reflects well (shear stress, temperature in the shear band, and velocity). The fluctuations of the reservoir were performed to stabilize the landslide as can be seen in the data, where the landslide started accelerating the reservoir level decreased in order to stop the acceleration. However, when they performed the last decrease of the reservoir, they could not stop the acceleration of the sliding mass due to the shear stress (i.e. Gruntfest number) and the temperature in the shear band crosses the stable values of the system (Figure 5B), making it impossible to stop the landslide.

Seeing the results of Figure 5, the critical temperature of the shear band has been found at 23.5°C. By reviewing the history of the landslide, we can see that the landslide did not collapse in the first embankment of the reservoir because the temperature in the shear band (22.9°C) did not overcome the critical temperature. However, during the second embankment (Figure 5A), the temperature at the shear band had already overcome the critical temperature, resulting in a blowup (collapse of the landslide) despite the last reduction of the reservoir. The last reduction of the reservoir started when the temperature at the shear band was at 24.8°C, thus overcoming the critical temperature makes impossible to stop the acceleration of the landslide.

5 Case of study: Shuping landslide

The Shuping landslide (Figure 6B) is also an ancient landslide that reactivated upon the Three Gorges dam was constructed in June of 2003 and the artificial lake started filling up. The area around the dam is formed by sandy mudstone and muddy sandstone of the Triassic Badong formation, and because of this, there have been several landslides. This area has long periods of rain which also induces the reactivation of the landslides. The thickness of this slide is about 30-70 meters and with a total rock mass of $2.7x10^7$ m^3 (Figure 6C). For this case, has been seen that the landslide accelerated when the lake water level decreased, with the possibility of having a delayed effect between the rise of the lake water level and the rise of acceleration of the slide (Figure 6D).

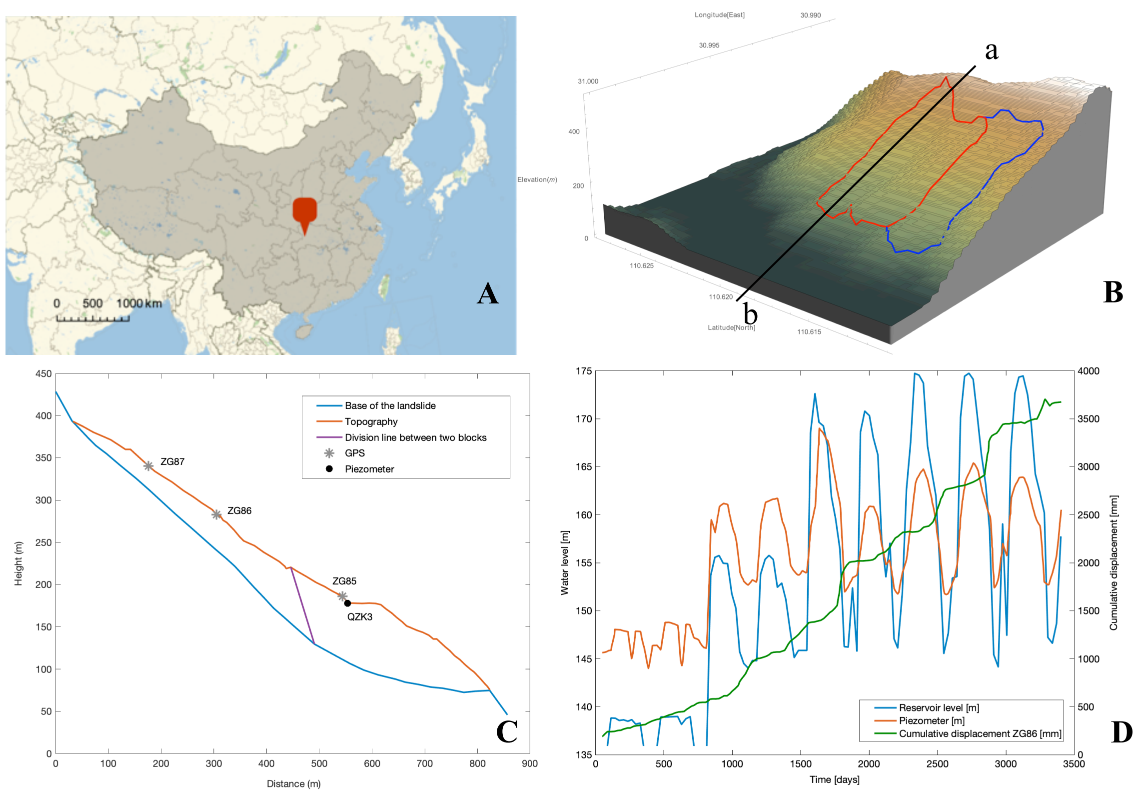

Figure 6. A) Map of location of the Shuping slide. **B)** 3D elevation map of the Shuping landslide (red is the active sector of the landslide and blue is the dormant sector of the landslide). **C)** Profile of the deep-seated Shuping landslide. **D)** Graph showing the variations of the reservoir level, the variations of the groundwater level from the piezometer QZK3, and the displacement from the GPS ZG86 during the 6 years of recorded data [*Yin et al, 2016*].

5.1 Geographical location and geological framework

The Shuping landslide is located nearby Xietanxiang village, in Zigui county in Eastern China. The slide occurred in the south crest of the valley where the Yangtze river flows along. Downstream the Yangtze river, at approximately 47km there is the Three Gorges Dam (Figure 6A).

The landslide is situated in the Southern part of the Shazhenxi anticline formed by mudstone, siltstone, and muddy limestone from the Triassic Badong formation. The layers of this formation in the south side of the anticline are dipping with an angle between 9 and 38° toward the direction of 120-173°. The top part of the landslide is formed by gravel, and the bottom part of the landslide is formed by clay and silty clay. The mass is sliding over a thin layer (0.6-1 m) of brown breccia soil and silty clay. And the underlying material of the landslide is composed by siltstone mixed with mudstone.

5.2 Groundwater analysis

To calculate the groundwater table for this case we used the transient method (Section 2.1) adding a diffusivity parameter (Equation 1) to fit the time lap that exists in the data between the variation of groundwater level and the displacement of the landslide (Figure 6D) [*Li, 2015*]. The boundary conditions chosen for this calculation have been the lake water level and the piezometer data that measured the groundwater level at QZK3 (see Figure 6C for location, *Wu et al, [2018]*).

As can be seen in Figure 6D, the groundwater level at the piezometer (QZK3) versus the lake water level is not constant (meaning that the piezometer level is not always above the lake level, as happens with Vaiont landslide). Therefore, in Figure 7A and 7B can be seen the groundwater profile for a low lake water level and for a high lake water level, respectively.

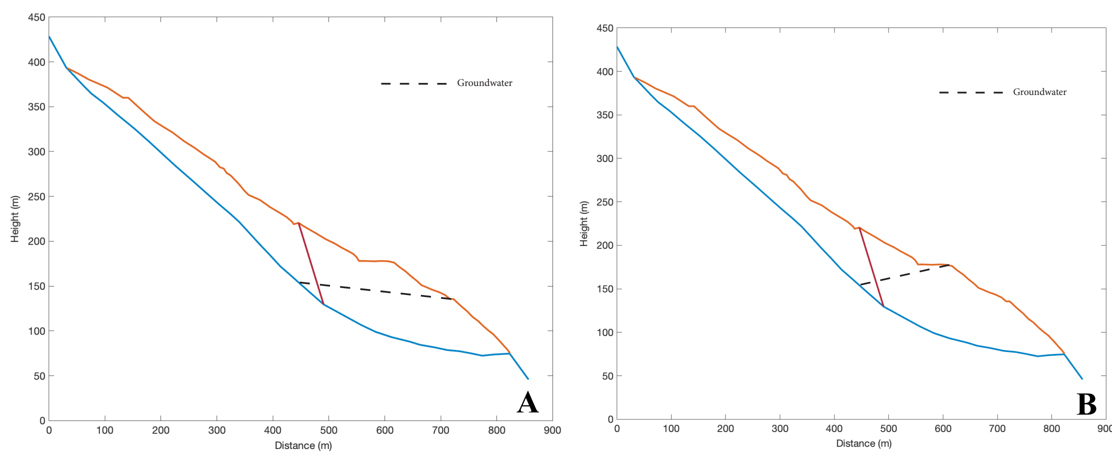

Figure 7. Profile of the Shuping landslide: **A)** Groundwater table when the reservoir level is at 135m. **B)** Groundwater table when the reservoir level is at 175m.

5.3 Shear stress results

In the case of Shuping landslide, we have enough data to straightforwardly calculate the shear stress for each lake level, without having to overestimate the basal shear stress value. In Figure 8 we plot the results of the shear stress calculated in MPa at each reservoir level (in meters) for each period of time (in days). The shear stress of the landslide varies between 1.12 and 1.2 MPa.

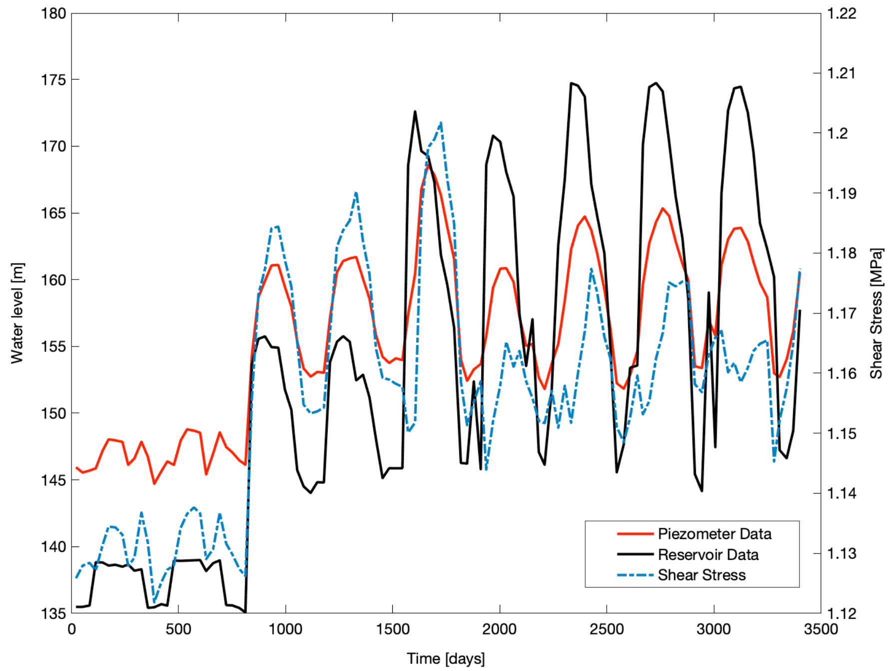

Figure 8. Graph showing the reservoir level, the piezometer data and the shear stress calculated for Shuping slide.

5.4 Transient stability analysis

In order to calculate the velocity of the landslide and the Gruntfest number, we need the material parameters of the clay that form the shear band of the Shuping landslide (Table 1). Some of these parameters have been taken from the Vaiont landslide [*Veveakis et al, 2007*] due to the absence of further information and the fact that the shear band of Shuping is formed by similar clays as in Vaiont.

In this study case, the system calculated for the Shuping landslide becomes unstable for a Gruntfest number of 0.88 and for a dimensionless ratio of temperature of 1.13 (Figure 9).

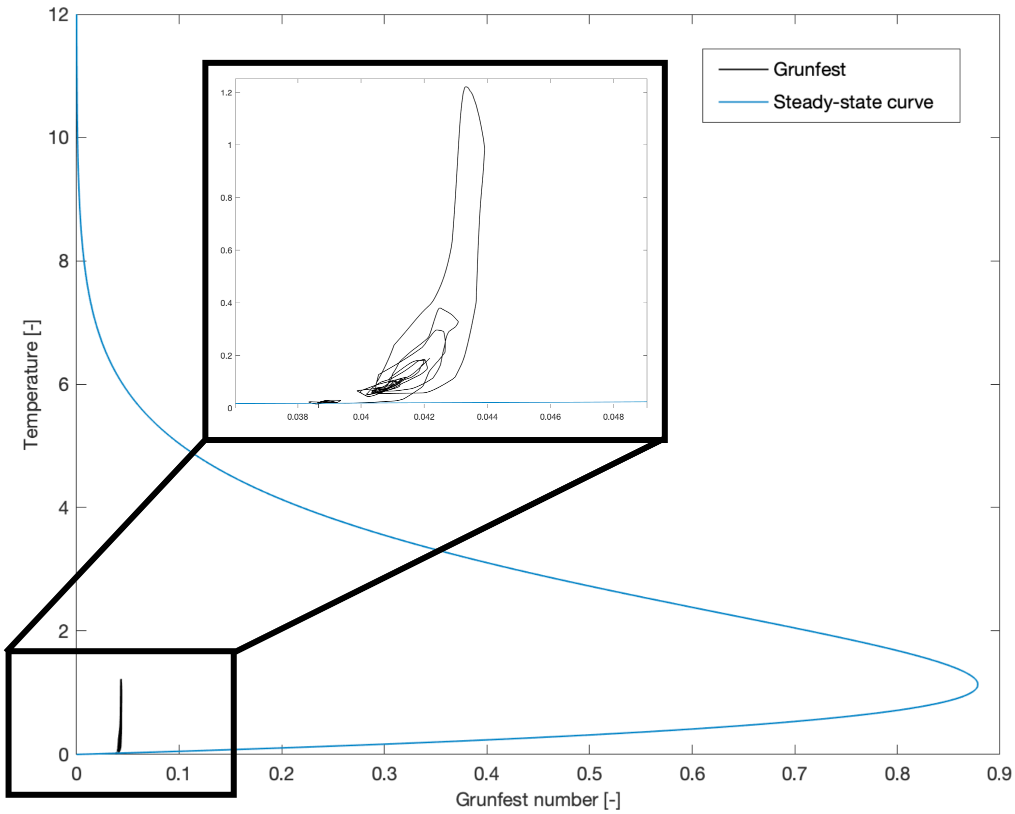

Figure 9. Gruntfest number calculated versus temperature, with the stability curve.

To calculate the velocity, we have chosen the GPS data from the station ZG86 (Figure 6C) because this station represents well the average displacement of the landslide, as the upper station ZG87 (Figure 6C) is located in an area that has been experiencing small localized slides. The same has happened with the station ZG85 (Figure 6C), located below ZG86. The velocity calculated for Shuping has been fitted for the field data [*Wu et al, 2018*]. In this case, for the velocity that we obtained with our calculations (Figure 10A) we needed to calculate two velocities to fit with more accuracy the velocity taken in the field (upper limit with strain-rate 1 and lower limit with strain-rate 2).

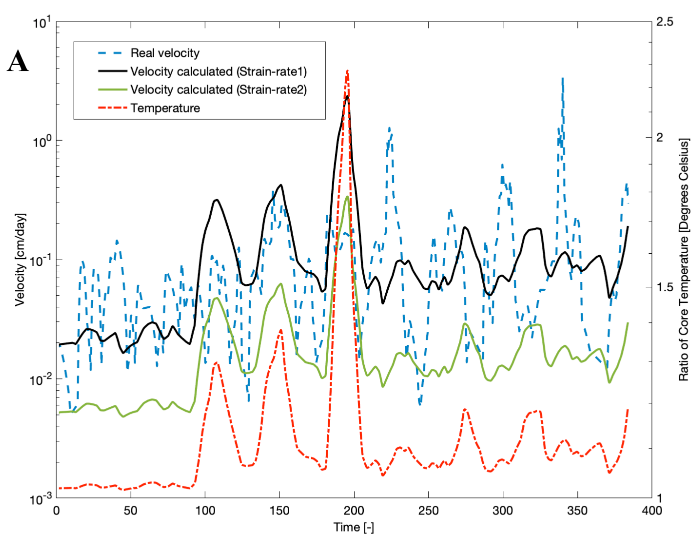

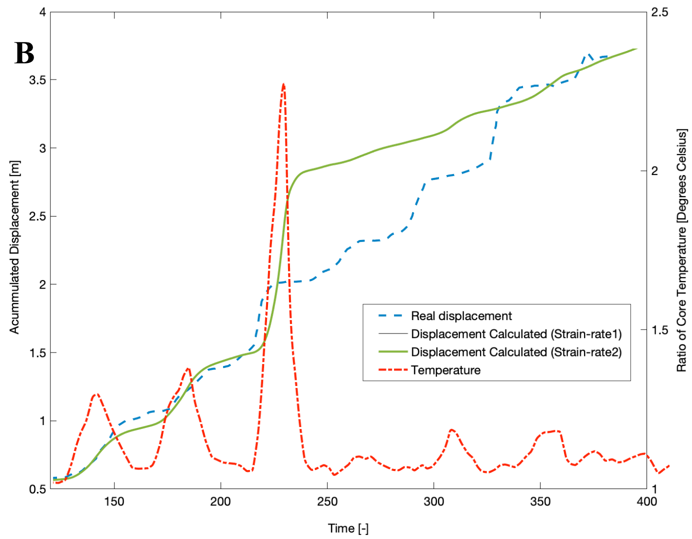

Figure 10. A) Velocity data from the field (calculated from the displacement obtained from [*Wu et al, 2018*]) as dashed line, two velocities calculated as lines, and dashed/dotted line indicating the ratio of the real temperature with the reference temperature in the shear band**. B)** Comparison of calculated (red and black lines), real displacements (blue dashed line), and ratio of temperature calculated (dashed/dotted line) in the shear band of Shuping landslide.

The temperature in this case (Figure 10A) is the ratio of the real temperature in the shear band over the reference temperature. Therefore, if we have a reference temperature from the field, we can obtain the real temperature in the shear band at any groundwater level (thus, reservoir and piezometer levels). Once the velocity is calculated, we convert our results to displacement and compare it to the displacement data from the field (Figure 10B) and to the temperature calculated in the shear band in order to understand the behavior of the gouge that causes the instability of the landslide.

The two different strain-rates applied to the calculations of velocity have been applied also to the displacements. Nevertheless, as Figure 10B shows, the different values of strain rate in the displacement do not affect the results of displacement. As it can be seen in Figure 10B, the model fits well the real data for the three first displacements, after that, the displacement increases smoother, due to the general behavior of the life of the reservoir. This behavior is well represented in the shear stresses calculated (Figure 10B) and in the temperature of the gouge (Figure 8) due to the fact that the three first cycles of the reservoir embankment are sharper in terms of the shear stress due to the loads of the groundwater level in the landslide. After these three reservoir embankments, the shear stress varies in a smoother way. It can therefore be seen that the results of the applied model are consistent with the data and fit well the field data, taking into account that we are fitting 10 years of very irregular data. Furthermore, the results show that the behavior of the landslide (high displacements) is consistent with the temperature in the shear band and the shear stresses calculated.

In general terms, can be seen in Figure 8 that the Shuping landslide has two distinctly different behaviors; one that is more unstable for the first 1800 days (Figure 10B, see the values of temperature of the shear band) where the shear stresses and displacements are higher because the groundwater table behaves as a steady state (Figure 7A), and a second more stable mechanism for the last 1600 days (Figure 10B, see the values of temperature of the shear band) where the shear stresses and displacements are lower because the groundwater table behaves as a transient mechanism that depends on the permeability of the landslide and has an opposite slope to the shear band and topography (Figure 7B).

6 Summary and Conclusions

The analysis performed in this study examined the claim that the point where physics inside the basal shear zone become unstable, corresponds to a point where the stability of the slide changes, making any attempt to stop the slide to seem inapplicable (case of Vaiont). The cases of Vaiont and Shuping landslides were studied in this paper. For both cases, the implementation of time-dependent shear stress in the thermal model presented in *Veveakis et al* [*2007*] paper, allowed to reproduce the history of the Vaiont and Shuping slides and combine the two main mechanisms that govern the behavior of a slide; the friction at the base of the slide and the pore pressure (thus the shear stress) evolution due to groundwater table variations. The analysis of the Vaiont landslide revealed that indeed the point where the heat dissipation process starts localizing is a critical point of the landslide. While for the Shuping landslide, we found an approximated point where the slide would become unstable and catastrophic.

In the model we implemented in this study we modified the rate sensitivity parameter N in order to fit the velocity/displacement "jumps" of the real data. Once the parameter N has been found, we adjusted the value of the parameter m to calculate the Gruntfest number (i.e. the shear stresses) for the stability of the landslide. In the case of Vaiont, we know that the landslide collapses after the last embankment of the reservoir, thus the Gruntfest number crosses the steady state curve making the system become unstable. However, for the Shuping landslide, the instability point is uncertain due to the landslide has not collapsed yet. Thus, we had chosen a value of N that fits as close as possible the real data (i.e. displacement), and the maximum value of m that keeps the system stable (as a larger value of m will change the system to unstable). Due to the previous facts, it is necessary to perform laboratory test of the clays located in the shear band of the landslide to get more information about the thermal sensitivity of these clays, thus we could get a better approximation of the critical Gr number required for the landslide to become unstable.

In conclusion, we have shown here that the physical mechanism of heat production due to the friction at the base of the slide managed to reproduce with accuracy the observed behavior of the sliding rock mass, as well as the variations of the reservoir water level that were performed in order to control the slide in both cases of study. Since even nowadays the mechanisms of giant, deep seated landslides remain unknown, and failure usually seems to occur without warning [*Kilburn and Petley, 2003*], the described mechanism could be used as an indicative criterion for the time up to which precautions should be taken in order to arrest a deep-seated slide. Indeed, complementing relative models (e.g. *Petley et al* [*2005*], *Helmstetter et al* [*2003*], *Sornette et al* [*2004*], *Voight* [*1988*]) with energetic considerations may provide useful insights on the mechanisms that govern these giant movements.

Acknowledgments

References

Alevizos S., Poulet T. and Veveakis, E., 2014. Thermo-poro-mechanics of chemically active faults. 1: Theory and steady-state considerations, *J. Geophys. Res. Vol 119 (6), 4558-4582, doi: 10.1002/2013JB010070,*

Alonso, E., (1989). Análisis de la estabilidad de taludes. Casos simples. En Corominas, J. (editor), "Estabilidad de Taludes y Laderas Naturales", Monografía n° 3, Sociedad Española de Geomorfología, pp. 97-118. (In Spanish)

Alonso, E., (1989). Métodos generales de equilibrio límite. En Corominas, J. (editor), "Estabilidad de Taludes y Laderas Naturales", Monografía n° 3, Sociedad Española de Geomorfología, pp. 119-166. (In Spanish)

Alonso, E. E., Pinyol, N. M. (2010). Criteria for rapid sliding I. A review of Vaiont case, Engineering Geology, 114, 198-210.

Anderson, D. L. (1980), An earthquake induced heat mechanism to explain the loss of strength of large rock and earth slides, in Proceedings of the International Conference on Engineering for Protection from Natural Disasters, pp. 569-580, John Wiley, New York.

Cecinato, F., Zervos, A., Veveakis, E. (2011). A thermo-mechanical model for the catastrophic collapse of large landslides, Int. J. Numer. Anal. Meth. Geomech., 35, 1507-1535.

Chan, T.F.C., Keller, H.B., 1991. Arc-length continuation and multi-grid techniques for nonlinear elliptic eigenvalue problems. SIAM J. Sci. Stat. Comput. 3 (2), 173-194.

Craig, R.F., 2004. Craig's Soil Mechanics. Seventh edition. ISBN 0-203-49410-5.

Dykes, A.P., Bromhead, E.N. (2018a). The Vaiont landslide: re-assessment of the evidence leads to rejection of the consensus, Landslides, 15, 1815-1832.

Dykes, A.P., Bromhead, E.N. (2018b). New, simplified and improved interpretation of the Vaiont landslide mechanics, Landslides, 15, 2001-2015.

Ferri, F., Di Toro, G., Hirose, T., Han, R., Noda, H., Shimamoto, T., Quaresimin, M., De Rossi, N., (2011). Low- to high-velocity frictional properties of the clay-rich gouges from the slipping zone of the 1963 Vaiont slide, northern Italy. Journal of Geophysical Research, Vol. 116, B09208.

Gruntfest, I. J., (1963). Thermal Feedback in Liquid Flow: Plane Shear at Constant Stress, Trans. Soc. Rheology, 7, 195-207.

Habib, P., (1967). Sur un mode de glissement des massifs rocheaux, C.R. Acad. Sci., 264, 151-153. (In French)

Hendron, A.J., Patton, F.D. (1985). The Vaiont slide, a geotechnical analysis based on new geologic observations of the failure surface, Technical Report GL-85-5. Washington, DC, Department of the Army US Corps of Engineers.

Kilburn, R.J.C. and Petley, D.M., (2003). Forecasting giant, catastrophic slope collapse: lessons from Vajont, Northern Italy, Geomorphology, 54, 21-32.

Lachenbrunch, A. H. (1980). Frictional heating, fluid pressure and the resistance to fault motion. J. Geophys. Res. 85, 6097-6112.

Li, Y., (2015). Mechanism of Landslides around China's Three Gorges Dam. Master Thesis. University of Alberta, Department of Civil and Environmental Engineering.

Mase, C.W. and Smith L. (1984). Pore-fluid pressures and frictional heating on a fault surface, PAGEOPH, Vol. 122 (2-4), 583-607, doi: 10.1007/BF00874618.

Muller, L., (1964). The rock slide in the Vaiont valley, Felsmech. Ingenoirgeol., 2, 148-212.

Muller, L., (1968). New considerations on the Vaiont slide, Felsmech. Ingenoirgeol., 6, 1-91.

Petley, D.N., Mantovani, F., Bulmer, M.H., Zannoni, A., (2005). The use of surface monitoring data for the interpretation of landslide movement patterns. Geomorphology, 66, 133-147.

Pinyol, N. M., Alonso, E.E. (2010). Criteria for rapid sliding II. Thermo-hydro-mechanical and scale effects in Vaiont case, Engineering Geology, 114, 211-227.

Poulet T., Veveakis E., K. Regenauer-Lieb, D.A. Yuen, 2014. Thermo-Poro-Mechanics of chemically active creeping faults. 3: The role of Serpentinite in Episodic Tremor and Slip sequences, and transition to chaos, *J. Geophys. Res. Vol 119 (6), 4606-4625, doi: 10.1002/ 2014JB011004.*

Rice, J., (2006). Heating and weakening of faults during earthquake slip, J. Geophys. Res., 111, B05311, doi: 10.1029/200JB004006.

Semenza, E. and Melidoro, E. (1992). Proceedings of the meeting on the 1963 Vaiont landslide. IAEG Italian Section and Dip Sci Geologiche e Paleontologiche, University of Ferrara, Publ 1, pp 1-218.

Tika, T.E., Hutchinson, J.N. (1999). Ring shear tests on soil from the Vaiont landslide slip surface, Géotechnique, 49, 59-74.

Vardoulakis, I., (2002a). Dynamic thermo-poro-mechanical Analysis of Catastrophic Landslides, Géotechnique, 52, 157-171.

Vardoulakis, I., (2002b). Steady shear and thermal run-away in clayey gouges, Int, J. Solids Struct., 39, 3831-3844.

Veveakis, E., Vardoulakis, I., and Di Toro, T., (2007). Thermoporomechanics of creeping landslides: The 1963 Vaiont slide, northern Italy. J. Geophys. Res., 112, F03026, doi: 10.1029/2006JF000702.

Veveakis, E., Alevizos, S., Vardoulakis, I., (2010). Chemical reaction capping of thermal instabilities during shear of frictional faults, Journal of the Mechanics and Physics of Solids, 58, 1175-1194.

Veveakis E., Poulet T. and Alevizos S, 2014. Thermo-poro-mechanics of chemically active faults. 2: Transient Considerations, *J. Geophys. Res. Vol 119 (6), 4583-4605 doi: 10.1002/2013JB010071.*

Veveakis, E. and Regenauer-Lieb, K., (2015). Cnoidal waves in solids, Journal of the Mechanics and Physics of Solids, 78, 231-248.

Voight, B., and Faust, C., (1982). Frictional heat and strength loss in some rapid landslides, Géotechnique, 32, 43-54.

Wu, Q., Tang, H., Ma, X., Wu, Y., Hu, X., Wang, L., Criss, R., Yuan, Y., Xu, Y., (2018). Identification of movement characteristics and casual factors of the Shuping landslide based on monitored displacements. Bulletin of Engineering Geology and the Environment. Doi:10.1007/s10064-018-1237-2.

Yin, Y., Huang, B., Wang, W., Wei, Y., Ma, X., Ma, F., (2016). Reservoir-induced landslides and risk control in Three Gorges Project on Yangtze River, China. Journal of Rock Mechanics and Geotechnical Engineering, 8, 577-595.